Research Article

For reprint orders, please contact: reprints@futuremedicine.com

Nanomedicine

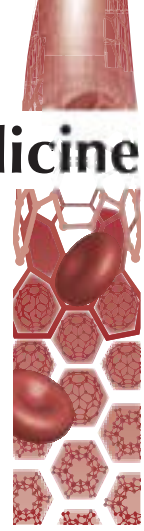

Uptake mechanism of metabolic-targeted gold nanoparticles

Tamar Dreifuss[1], Tal-Shachar Ben-Gal[1], Katerina Shamalov[2], Aryeh Weiss[1], Avi Jacob[2], Tamar Sadan[1], Menachem Motiei[1] & Rachela Popovtzer*[,1]

[1]Faculty of Engineering & the Institutes of Nanotechnology & Advanced Materials, Bar-Ilan University, Ramat-Gan, Israel

[2]The Mina & Everard Goodman Faculty of Life Sciences, Bar-Ilan University, Ramat-Gan, Israel

*Author for correspondence: rachela.popovtzer@biu.ac.il

Aim: To elucidate the interactions, uptake mechanisms and cytotoxicity profile of glucose-functionalized gold nanoparticles (2GF-GNPs), for expanding and advancing the recently proposed technology of metabolic-based cancer detection to a variety of cancer diseases. **Methods:** Several cell types with different metabolic features were used to assess the involvement of GLUT-1 and different endocytosis pathways in 2GF-GNP uptake, and the cytotoxicity profile of 2GF-GNPs. **Results:** Cellular uptake of 2GF-GNP strongly correlated with GLUT-1 surface expression, and occurred mainly through clathrin-mediated endocytosis. 2GF-GNPs showed no toxic effect on cell cycle and proliferation. **Conclusion:** These findings promote development of metabolic-based cancer detection technologies, and suggest that 2GF-GNPs may enable specific cancer detection in a wide range of tumors characterized by high GLUT-1 expression.

First draft submitted: 17 January 2018; Accepted for publication: 5 April 2018; Published online: 20 July 2018

Keywords: cancer • clathrin-mediated endocytosis • glucose-coated nanoparticles • GLUT-1 • gold nanoparticles • metabolic-targeting

Over the past decade, great efforts have been invested in fabrication of nanomaterials that can improve the diagnosis and treatment of cancer. A variety of biomolecules are typically incorporated within nanomaterials to achieve therapeutic abilities, or used as coating elements for active tumor targeting [1–4]. Carbohydrates are among the most widespread biomolecules in living systems. Their important multifaceted roles in many biological processes, together with their polyvalency, biocompatibility and small size, make them an advantageous component for incorporation in nanobiosystems [5]. The most common simple carbohydrate, and the primary source of metabolic energy in human cells, is glucose. Glucose-functionalized nanomaterials are emerging as a highly effective technique for specific tumor targeting [6], by exploiting the Warburg effect – the increased glucose consumption and glycolysis rate of tumor cells [7].

We have recently developed glucose-functionalized gold nanoparticles (GF-GNPs), utilized as metabolically targeted computed tomography (CT) contrast agents [6]. We demonstrated, both *in vitro* and *in vivo*, that the coating glucose molecules were recognized by head and neck cancer cells (A431) only when conjugated to GNP through their second carbon position (2GF-GNP), leading to significant uptake by the highly metabolically active head and neck tumor but not by highly metabolically active inflammatory regions, due to dissimilarities in angiogenesis occurring under different pathologic conditions. This, in contrast to the prevalently used ^{18}fluorodeoxyglucose-PET imaging technique, which cannot distinguish between cancer and inflammation (Figure 1) [6]. Thus, 2GF-GNPs provide a solution for specific tumor cell targeting, and thereby sensitive tumor detection and precise differentiation between cancer and inflammatory processes, with CT imaging. In addition, several recent studies have demonstrated *in vitro* the feasibility of different glucose-coated nanoparticles as tumor targeting agents [8–11]. However, the underlying mechanism responsible for the uptake and functionality of glucose-coated particles is still not fully understood.

Cellular uptake of endogenous glucose molecules is mainly associated with GLUT-1 [12–14]. However, because glucose-functionalized nanomaterials are considerably larger than the small glucose molecule, additional mechanisms are likely involved in cellular uptake. Extensive evidence shows that uptake of nanoparticles by cellular systems can occur through various endocytosis pathways [15–18]. Moreover, according to some reports [17,19,20], the

Future Medicine

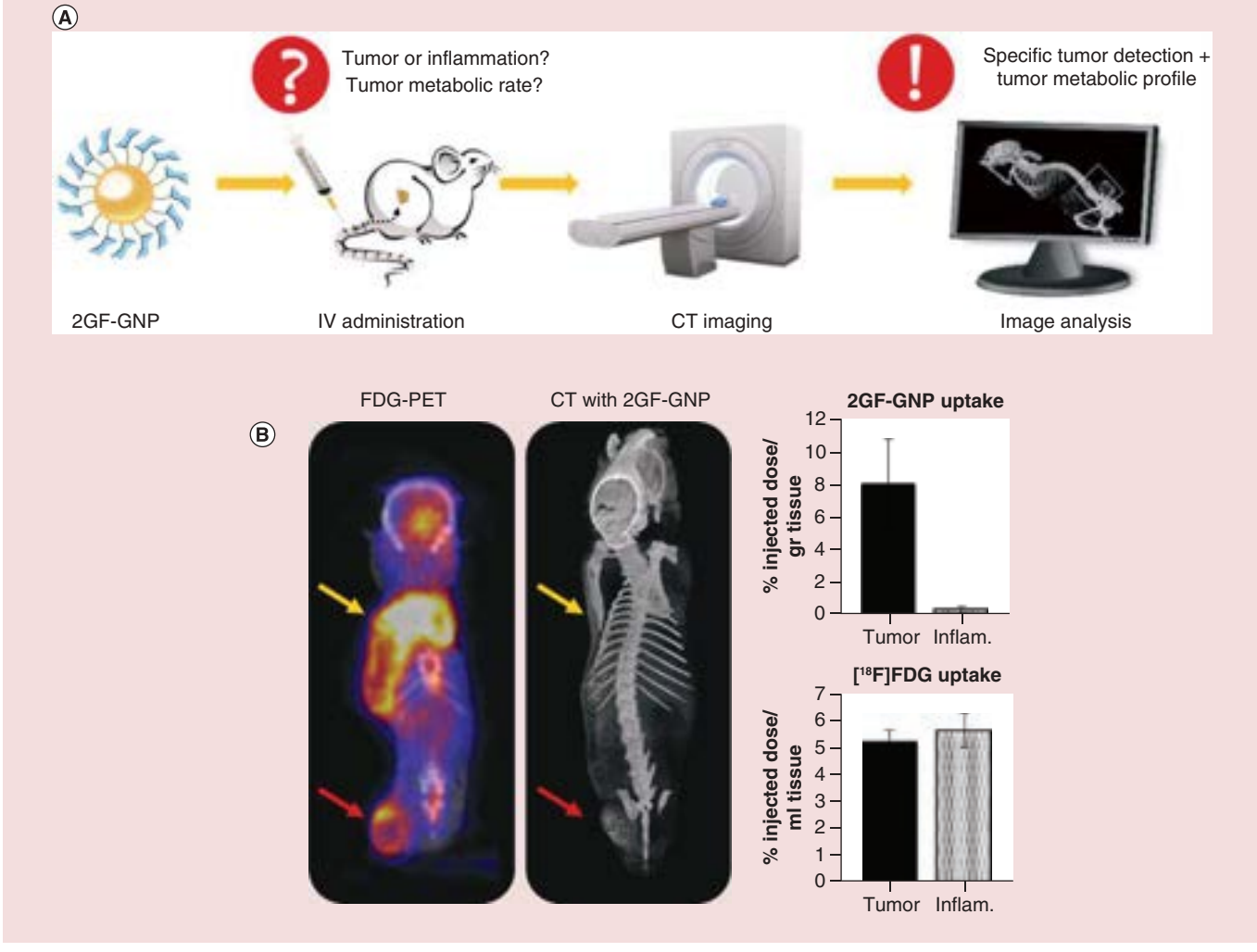

Figure 1. Glucose-functionalized gold nanoparticles as a metabolic-targeted computed tomography contrast agent for specific tumor detection. (A) Schematic diagram of the glucose-functionalized gold nanoparticles (2GF-GNPs) based imaging process. 2GF-GNPs are intravenously injected into a combined tumor-inflammation mouse model, followed by computed tomography (CT) scan. This strategy enables specific tumor detection, based on the tumor metabolic profile, and distinguishes the tumor from metabolically active inflammation processes. **(B)** 2GF-GNP-based technology shows superior abilities compared with commonly used fluorodeoxyglucose-PET. Both CT imaging and quantitative Au measurements show clear distinction between tumor and inflammation, in contrast to fluorodeoxyglucose-PET, which shows neither visible nor quantitative differentiation between the two.
Adapted with permission from [6] © ACS Publications (2016).

same nanoparticle can show different endocytosis pathways in different cell types. Each endocytic pattern results in distinct internalization and intracellular fate. Endocytosis through clathrin-coated pits (receptor-mediated) or uncoated pits (fluid phase) leads to the lysosome, while caveolae-mediated endocytosis translocates the substances to the endoplasmic reticulum, Golgi or passage through the cell by trancytosis [16,21]. Hence, understanding the underlying uptake patterns of metabolic-targeted glucose-functionalized nanoparticles, as well as elucidating their cytotoxicity profile, is essential for advancing their future clinical use as specific tumor imaging agents.

To this aim, we performed a comprehensive *in vitro* study examining cytotoxicity and potential uptake mechanisms of 2GF-GNPs in cancer cell lines with different metabolic profiles, exhibiting high or low GLUT-1 expression. We found a significant dependence of 2GF-GNP uptake on GLUT-1 overexpression, as well as a strong correlation between GLUT-1 surface expression and clathrin-mediated endocytosis of the particles. This indicates that interaction between 2GF-GNPs and GLUT-1 serves to trigger particle endocytosis through the clathrin-mediated pathway. Moreover, 2GF-GNPs were found to have no cytotoxic effect on the various cell lines. These findings

are critical for further promoting the technology of metabolic-based cancer detection and differentiation between tumor and inflammation (Figure 1) to clinical application.

Methods

GF-GNP synthesis & characterization

Synthesis of 20 nm spherical GNPs was carried out on the basis of Enüstün & Turkevic's methodology [22]. A total of 414 µl of 50% w/v $HAuCl_4$ solution was added to 200 ml purified water, followed by heating in an oil bath until boiling. Then, 4.04 ml of 10% solution of sodium citrate tribasic dihydrate (Sigma-Aldrich, Rehovot, Israel) were added, followed by 10 min stirring. After cooling to room temperature, 120 µl of 50 mg/ml PEG7 solution (O-(2-Carboxyethyl)-O′-(2-mercaptoethyl) heptaethylene glycol) (Sigma-Aldrich) were added, and the solution was stirred for 4 h. The, the solution was centrifuged to get rid of excess PEG7. Following centrifugation, 200 µl of 10 mg/ml 1-Ethyl-3-(3-dimethylaminopropyl) carbodiimide HCl (EDC) solution (Thermo Scientific) and 200 µl of 10 mg/ml N-Hydroxysulfosuccinimide sodium salt (NHS) solution (Sigma-Aldrich) were added. The following glucosamine molecules were used for glucoseamine conjugation: b-D-Glucopyranosyl amine (Carbosynth) and 2-Amino-2-deoxy-D-glucose HCl (Sigma-Aldrich). Each of these glucosamine molecules was added individually in excess to yield 1GF-GNP and 2GF-GNP, respectively. The nanoparticles solution was centrifuged until a final Au concentration of 30 mg/ml [3,6,23,24]. Characterization of GF-GNPs was performed using transmission electron microscopy (TEM, JEM-1400, JEOL), ζ potential (ZetaSizer 3000 HS; Malvern Instruments, Malvern, UK) and dynamic light scattering.

Cellular uptake experiments

Qualitative studies

Head and Neck squamous cell carcinoma (A431) cells, lung carcinoma (A549) cells and 3T3 fibroblast cells were cultured in 3 ml Dubleco's Modified Eagle's Medium containing 5% FCS, 0.5% Penicillin and 0.5% Glutamine. Prostate adenocarcinoma (LNCaP; lymph node carcinoma of the prostate) cells were cultured in 3 ml Roswell Park Memorial Institute medium containing 5% FCS, 0.5% Penicillin and 0.5% Glutamine. For fluorescence microscopy experiments, 10 µl of fluorescent-coated (Rhodamine B, Sigma, Israel) 2GF-GNPs were added to the medium for 30 min at 37°C and cells were imaged using live imaging microscopy (Axio Observer Z1). Images were taken at 10 min. For live streaming of cellular uptake, 2 µl of fluorescent-coated 2GF-GNPs were added to A431 cells. Imaging was conducted over 10 min incubation, and Fiji (ImageJ) was used for video analysis. Expanded information can be found in the Supplementary Methods.

Quantitative studies

Quantitative uptake experiments were carried out for all cell types (A431, A549, LNCaP and 3T3). A total of 0.3 mg of 1GF-GNPs or 2GF-GNPs were added to the medium, following by 30-min incubation at 37°C. Each experimental group consisted of three samples, 2×10^6 cells each. After incubation, the medium was removed and cells were washed twice with PBS, followed by trypsin treatment. The cells were centrifuged twice and finally, aqua-regia acid (a mixture of nitric acid and hydrochloric acid in a volume ratio of 1:3) was added to the cells for atomic absorption spectroscopy (flame atomic absorption spectroscopy, FAAS) gold detection.

Atomic absorption spectroscopy analysis

Atomic absorption spectroscopy (AA 140; Agilent Technologies, CA, USA) was used to determine gold concentrations in the investigated samples. Cell samples were dissolved in 100 µl aqua regia acid and diluted with purified water to a total volume of 3 ml. After filtration, gold concentrations were determined according to absorbance values, with correlation to calibration curves.

GLUT-1 inhibition test

For GLUT-1 inhibition, cells (all types mentioned above) were preincubated with cytochalasin B (Cayman Chemical) for 2 h at 100 µg/ml final concentration, based on previous studies which showed that this concentration can induce efficient GLUT-1 inhibition without affecting cell viability [6,25]. Then, the medium was removed and the cells were washed twice with PBS before adding the GNPs. Incubation with GNPs was performed for 30 min at 37°C, followed by trypsin treatment and quantitative FAAS analysis. In addition, qualitative scanning

electron microscope (SEM) images were taken for A431 cells after incubation with 2GF-GNPs, with or without CB treatment.

Endocytosis inhibition

Endocytosis was first inhibited by preincubating of the cells for 30 min at 4°C, followed by incubation with 2GF-GNPs for 30 min at 4°C. In addition, to investigate the endocytosis pathway of 2GF-GNP internalization, cells were preincubated for 1 h at 37°C with the following inhibitors individually, at concentrations which efficiently inhibit endocytic pathways, with no toxic effect on the cells, based on prior literature [16,26]: 7 μg/ml of chlorpromazine hydrochloride (Sigma) to inhibit the clathrin- mediated endocytosis, 25 μg/ml of nystatin (Sigma) to inhibit caveolae-mediated endocytosis, or 50 μM amiloride hydrochloride (Sigma) to inhibit macropinocytosis. Following preincubation with the inhibitor solutions, the medium was removed and freshly prepared medium containing 2GF-GNPs and inhibitors at the same concentrations was added for further 30 min incubation. Cell samples that were treated with 2GF-GNPs but without inhibitors were used as control, and their uptake was expressed as 100%.

Flow cytometry for detection of GLUT-1 surface expression

Flow cytometry was applied to investigate the expression levels of GLUT-1 on the surface of the various cell lines. For surface staining, cells were incubated with GLUT-1 primary antibody (R&D Systems) at 4°C for 30 min in buffer made of PBS and 2% BSA. Then, cells were washed with buffer solution followed by 30 min incubation with secondary antibody Alexa488 (Jackson) in the dark at 4°C. In order to detect non-specific staining, controls stained with only secondary antibody were used. Cells were analyzed on a FACSAria III flow cytometer. Mean fluorescence intensity (MFI) derived from fluorescence histogram was used to study the level of cell surface GLUT-1 expression. For comparison between the different cell lines, delta MFI (dMFI) was calculated as dMFI = $(MFI_{(GLUT\text{-}1)}-MFI_{(control)})/MFI_{(control)}$.

Scanning electron microscopy

A431 cells were seeded on glass coverslips and incubated with 2GF-GNPs for 30 min, with or without cytochalasin B (100 μg/ml final concentration). Following incubation, cells were washed twice with PBS and then fixed with karnovsky's fixative. After fixation, samples were incubated in 1% buffered osmium tetroxide for 90 min at 4°C. Samples were dried with 30, 50, 75 and 95% ethanol, and then absolute ethanol. Images were taken using scanning electron microscope (Inspect, FEI) in secondary electron (SE) mode and high contrast back-scattered electron (BSE) mode.

Cytotoxicity experiments

Cells were incubated at 37°C with different amounts of 2GF-GNPs for 24, 48 and 72 h. Cell proliferation was studied at the different time points by hemocytometer-based cell quantitation with trypan blue viability assay. In addition, cell cycle analysis was performed for cells after 24-h incubation with 2GF-GNP using flow cytometry. Following incubation, cells were harvested and washed twice in cold PBS. Then, cells were fixed for 24 h at 4°C, using 4 ml cold ethanol (-20°C, 70%). For propidium-iodine (PI) staining and flow cytometric analysis, fixed cells were washed and centrifuged in 500 ×*g*, for 5 min. Cell pellet was then resuspended in 400 μl PBS supplemented with 8 μl RNAse (1 μg/ml) and 4 μl PI (2 μg/ml). Samples were incubated for 10 min in the dark before analyzed by flow cytometry.

Statistical analysis

One-way analysis of variance followed by Bonferroni's multiple comparison was performed for comparison between the different cell types or inhibitor treatments. Differences between two groups were analyzed using Student's *t*-test. Correlations were analyzed using Pearson's correlation coefficient.

Results & discussion

GF-GNP synthesis & characterization

We synthesized two types of GF-GNPs, 20 nm in diameter, coated with glucose via a PEG linker. The glucose molecule was covalently attached through different carbon atoms, C-2 or C-1, to yield 2GF-GNP and 1GF-GNP, respectively. This minor molecular difference has a substantial effect on the biological function of glucose-coated GNPs, as it has been previously demonstrated that position C-1, as opposed to C-2, is critically important for

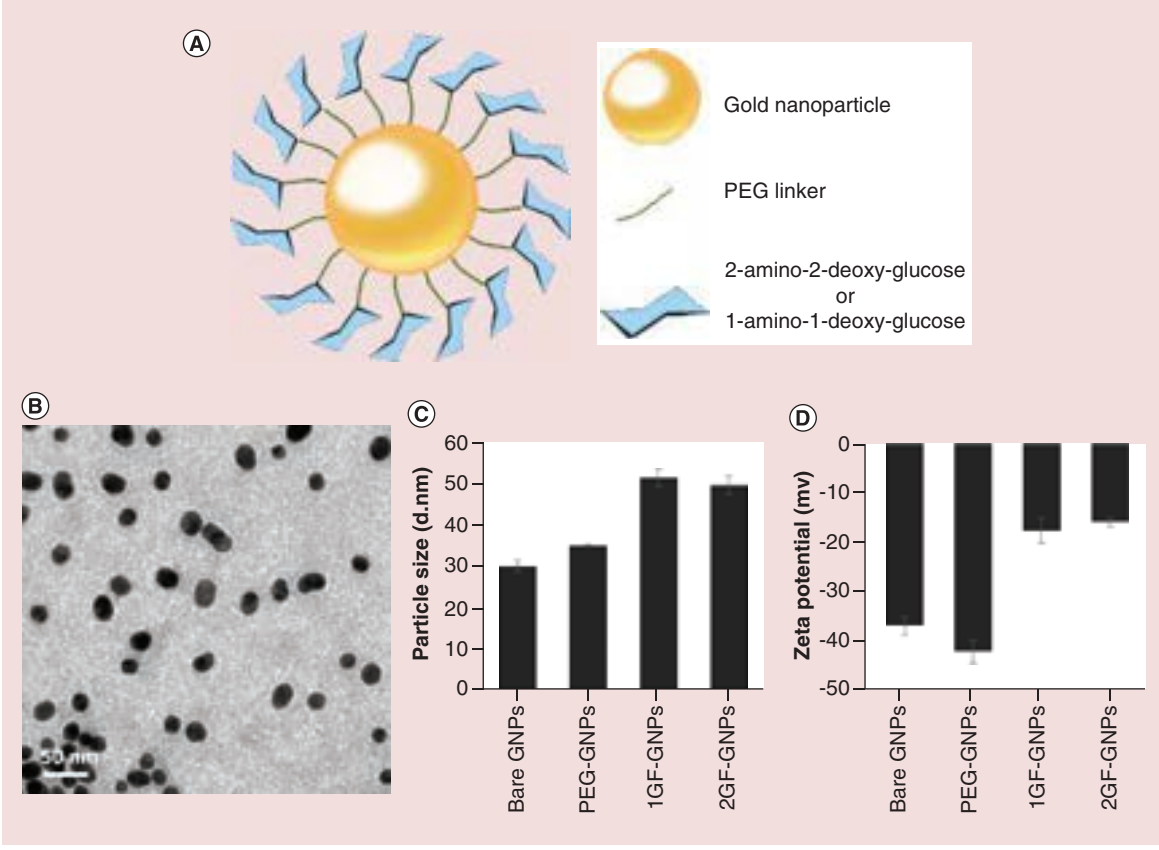

Figure 2. Glucose-functionalized gold nanoparticle characterization. (A) Schematic diagram of the glucose-functionalized gold nanoparticles (GF-GNPs), showing that they have the same physicochemical characteristic, and therefore differ only in their glucose conjugation site. **(B)** Transmission electron microscope image of gold nanoparticles with a mean diameter of 20 ± 3 nm. Scale bar: 50 nm. **(C)** Dynamic light scattering measurements (hydrodynamic diameter) of the GF-GNPs following each conjugation level. **(D)** ζ-potential measurements of the GF-GNPs following each conjugation level. Results presented as mean ± standard deviation.

glucose binding to GLUT-1 [6,27]. Thus, chemical conjugation to the GNP through this position (C-1) prevents the interaction with GLUT-1. Therefore, 1GF-GNP was utilized as a control particle for the quantitative experiments. The GF-GNPs were characterized using TEM, dynamic light scattering and ζ potential (Figure 2).

TEM showed that spherical, uniformly distributed GNPs at a diameter of 20 ± 3 nm were obtained. The increase in the hydrodynamic diameter and reduction of negative ζ potential following glucose conjugation confirmed the efficacy of the chemical coating, and demonstrated that the two GF-GNP types, while differing in their intramolecular glucose conjugation site, have the same physicochemical characteristics.

Cellular uptake of 2GF-GNPs

The uptake of GF-GNPs into cancer cells was examined in four different cell lines with different expression of GLUT-1: A431 head and neck squamous cell carcinoma, A549 non-small-cell lung carcinoma, LNCaP prostate adenocarcinoma and 3T3 fibroblasts. The first two are known for high GLUT-1 expression, while the latter two are known for low GLUT-1 expression [28–32].

First, we qualitatively examined the uptake of 2GF-GNPs (30 mg/ml, 10 ml), marked with Rhodamine B, into the different cell types. Fluorescence live cell microscopy showed that 2GF-GNPs were internalized into all four cell types, without penetrating the nuclei (Figure 3). Interestingly, cellular uptake was observed within seconds after incubation, and was essentially completed within 3 min (Supplementary Videos 1 & 2). Average fluorescence intensity in representative A431 cells over time is plotted in Figure 4 (based on the region of interest [ROI] set, Supplementary Figure 1), showing rapid internalization and stabilization of the signal within the cells.

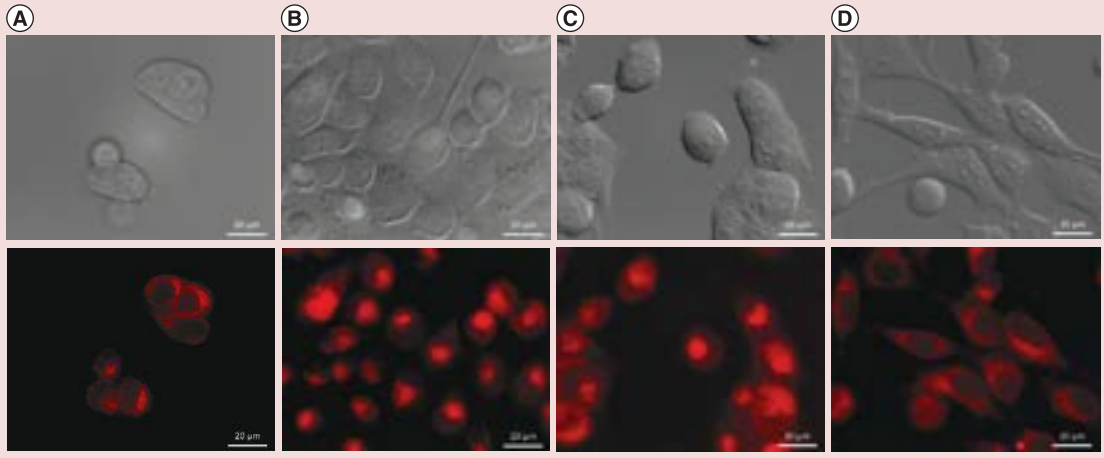

Figure 3. Cellular uptake of Rhodamine-B-conjugated 2-glucose-functionalized nanoparticles. Representative images of: **(A)** A431 cells; **(B)** A549 cells; **(C)** LNCaP cells; and **(D)** 3T3 cells treated with Rhodamine B 2-glucose-functionalized nanoparticles (10 min). Top: Bright field image of the cells. Bottom: Rhodamine B-conjugated 2-glucose-functionalized nanoparticles (red). Scale bar: 20 μm.

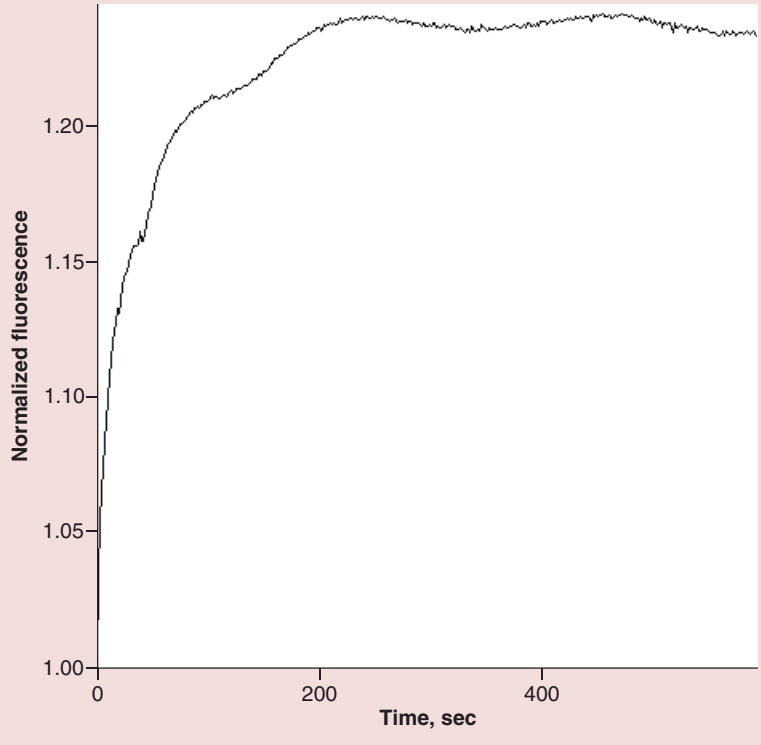

Figure 4. Kinetics of 2-glucose-functionalized nanoparticle uptake. Mean fluorescence intensity vs time in representative A431 cells. Mean intensity is normalized to intensity at the first time point.

The degree of GLUT-1 expression affects 2GF-GNP uptake

We next examined a possible correlation between 2GF-GNP uptake and GLUT-1 expression. GLUT-1 surface expression in the different cell types was evaluated by fluorescence-activated cell sorting, using GLUT-1 antibody.

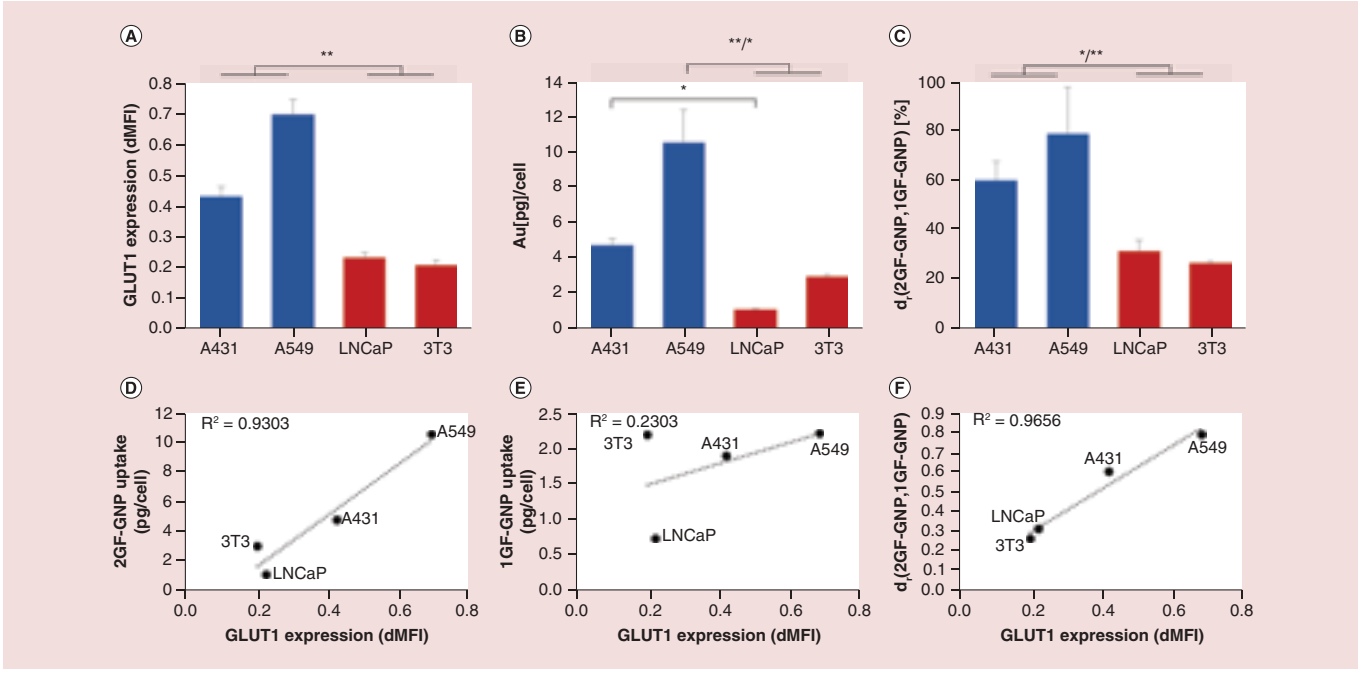

Figure 5. Glucose-functionalized gold nanoparticle uptake as a function of GLUT-1 expression. Glucose-functionalized gold nanoparticle (GF-GNP) uptake was examined in high GLUT-1-expressing cells (presented by blue bars) as compared with low GLUT-1-expressing cells (red bars). **(A)** GLUT-1 surface expression in the different cell types as measured by flow cytometry, using GLUT-1 antibody. **$p < 0.01$ for both A431 and A549 versus LNCaP and 3T3; one-way ANOVA followed by Bonferroni *post hoc*. **(B)** 2-Glucose-functionalized nanoparticle (2GF-GNP) uptake in the various cells, measured by flame atomic absorption spectroscopy. *$p < 0.05$, A431 versus LNCaP, and A549 vs 3T3; **$p < 0.01$ A549 vs LNCaP. **(C)** Relative difference between cellular uptake of 2GF-GNP and 1GF-GNP, defined as: $d_r = 100*(2GF\text{-}GNP\text{-}1GF\text{-}GNP)/2GF\text{-}GNP$. *$p < 0.05$, A431 versus LNCaP and 3T3, and A549 versus LNCaP; **$p < 0.01$ A549 vs 3T3. Results presented as mean ± scanning electron microscopy. **(D–F)** Correlation between GLUT-1 expression and **(D)** 2GF-GNP uptake, **(E)** 1GF-GNP uptake and **(F)** d_r(2GF-GNP,1GF-GNP).

Next, the cells were incubated with 2GF-GNPs for 30 min and gold concentrations were quantitatively determined by FAAS.

We found that GLUT-1 expression in A549 and A431 cells was significantly higher as compared with LNCaP and 3T3 cells ($p < 0.01$), with the highest GLUT-1 expression observed for A549 cells (Figure 5A). Cellular uptake of 2GF-GNP corresponded with these results, showing significantly higher uptake in the high-GLUT-1-expressing cells as compared with low GLUT-1-expressing cells ($p < 0.05$–0.01); the highest uptake was seen in A549 cells (Figure 5B). Uptake of 1GF-GNP was lower than that of 2GF-GNP in all cell lines (1.9 vs 4.8 pg/cell; 2.2 vs 10.6 pg/cell; 0.7 vs 1.1 pg/cell, and 2.3 vs 3 pg/cell for A431, A549, LNCaP and 3T3 cells, respectively). The relative difference (d_r) between uptake of 2GF-GNP and 1GF-GNP was calculated ($d_r = 100 \times (2GF\text{-}GNP\text{-}1GF\text{-}GNP)/2GF\text{-}GNP$), showing that d_r was significantly greater in GLUT-1-overexpressing cells (Figure 5C). This finding was consistent with the d_r observed in additional cell lines, PC3 prostate cancer cells and B16 melanoma cells, which are known for high GLUT-1 expression (Supplementary Figure 2) [32,33].

We further found a high correlation between 2GF-GNP uptake and GLUT-1 expression (Pearson's coefficient, $R^2 = 0.9303$), as well as between d_r and GLUT-1 expression ($R^2 = 0.9656$), while 1GF-GNP uptake showed very low correlation with GLUT-1 expression ($R^2 = 0.2303$) (Figure 5D, E & F). These results confirm the strong dependence of GF-GNP uptake on GLUT-1 expression, specifically when glucose is conjugated to GNP through the second carbon position. Interestingly, our results are in accord with other studies showing that cellular uptake of ^{18}FDG, which is also modified at the second carbon position, highly correlates with GLUT-1 expression [29,31].

To further examine the involvement of GLUT-1 in the binding and uptake process of 2GF-GNPs, cells were incubated with GF-GNPs after pre-incubation with Cytochalasin-B (CB; 100 µg/ml), a well-known GLUT-1 inhibitor [34,35].

First, the effect of CB on cell surface binding was examined using SEM, in cells with or without CB pre-treatment and 2GF-GNP incubation. Figure 6A presents cell morphology of representative A431 cells (using

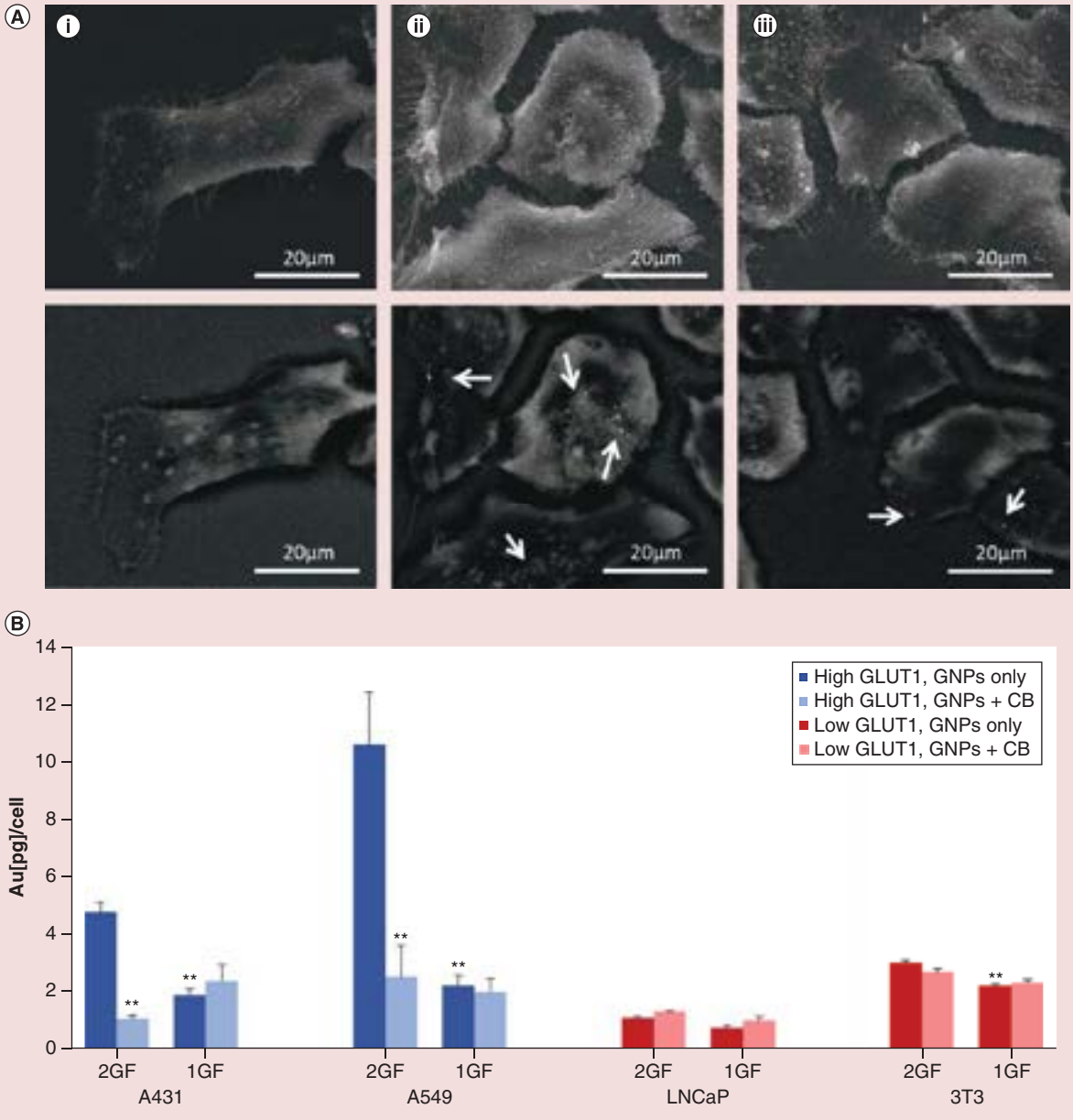

Figure 6. Effect of GLUT-1 inhibitor on glucose-functionalized gold nanoparticle uptake. (A) Scanning electron microscope (SEM) secondary electron (SE; top) images and back-scattered electrons (BSE; bottom) images of A431 cells **(i)** without 2-glucose-functionalized nanoparticles (2GF-GNPs); **(ii)** with 2GF-GNPs; **(iii)** with 2GF-GNPs after pretreatment with Cytochalasin-B (CB). The back-scattered-electron imaging images show gold nanoparticles as white dotted areas (indicated by arrows). Untreated cells show higher amounts of 2GF-GNPs on their surface as compared with cells pretreated with CB. **(B)** Cellular uptake of GF-GNPs with or without GLUT-1 inhibitor (CB), in high GLUT-1-expressing cells (blue bars) or low GLUT-1-expressing cells (red bars), as measured by flame atomic absorption spectroscopy. Results presented as mean ± SEM; n = 3. One-way analysis of variance followed by Bonferroni *post hoc*. **p < 0.01, A431 and A549 (high GLUT-1) with 2GF-GNPs versus CB treated cells or cells with 1GF-GNP; and 3T3 with 2GF-GNP versus 3T3 with 1GF-GNP.

secondary electron imaging) and GNPs in bright contrast upon the cells (using high-contrast backscattered-electron imaging). It was clearly visible that CB had a considerable effect on cell surface 2GF-GNP binding: In cells treated with 2GF-GNP only, clusters of gold are seen on the cell surface, while in cells pre-incubated with CB, only small amounts of gold are observed on the surface, probably due to GLUT-1 blocking which prevents the specific glucose-GLUT-1 interaction.

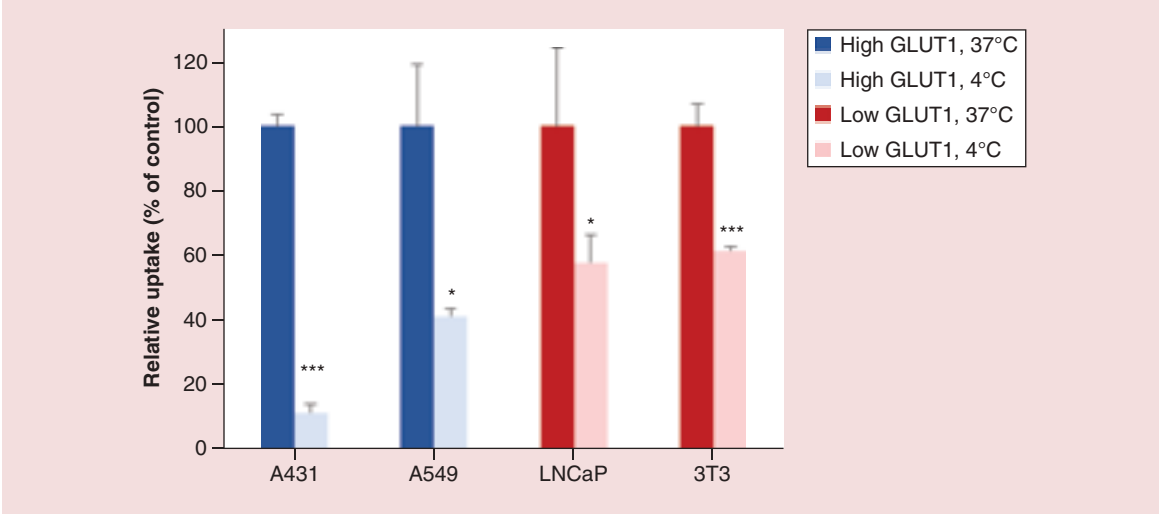

Figure 7. Effect of temperature on 2-glucose-functionalized nanoparticle uptake. 2-Glucose-functionalized nanoparticles (2GF-GNPs) were incubated with high (blue bars) or low (red bars) GLUT-1-expressing cells at either 37°C or 4°C. 2GF-GNP uptake was measured by flame atomic absorption spectroscopy. Low temperature significantly reduced 2GF-GNP uptake in all cell types, with high-GLUT-1 cells showing higher fold change in relative uptake. 2GF-GNP uptake at 37°C is expressed as 100% and defined as control. ***$p < 0.001$, *$p < 0.05$; Student's t-test. Results presented as mean ± standard error of the mean ($n = 3$).

To quantitatively measure the effect of GLUT-1 inhibition on gold uptake, we analyzed gold amounts in cells after CB pretreatment, using FAAS. Our results show that CB pretreatment significantly inhibited uptake of 2GF-GNP into high-GLUT-1 A431 and A549 cells ($p < 0.01$), but had no effect on 2GF-GNP uptake into low-GLUT-1 LNCaP and 3T3 cells. Likewise, as opposed to 2GF-GNP, uptake of the control particle 1GF-GNP which is unable to interact with GLUT-1, was not affected by CB in all cell lines, demonstrating its nonspecific cellular uptake (Figure 6B).

GLUT-1 triggers clathrin-mediated endocytosis of 2GF-GNP

Despite the specific interaction between 2GF-GNP and GLUT-1, we assumed that the large size of 2GF-GNP, as compared with a simple glucose molecule, prevents its direct transport across the membrane via GLUT-1. Additionally, previous TEM images of A431 cells after incubation with 2GF-GNP showed accumulation of well-defined nanoparticles inside an endosome [6]. Therefore, we hypothesized that 2GF-GNP internalization might be completed by a second step, probably endocytosis.

In contrast to simple diffusion or the facilitated diffusion through GLUT-1, endocytosis is an energy-dependent process. Therefore, we first conducted temperature-dependence experiments to examine the effect of impediment of endocytic pathways. Cells were incubated with 2GF-GNP for 30 min at either 37or 4°C, and gold concentrations were then quantitatively measured by FAAS. We found that significant, but not full reduction in 2GF-GNP uptake occurred in all cell types at a low temperature of 4°C as compared with 37°C, demonstrating a basal passive uptake of 2GF-GNP in all cells. However, a more robust reduction effect can be seen in the high-GLUT-1 cells, A431 and A549 ($p < 0.05$, $p < 0.001$; Figure 7), suggesting that a lower percentage of passive transport occurs in these cells, probably due to the higher degree of specific interactions with GLUT-1.

As cellular processes other than endocytosis, such as diffusion, are also impeded at low temperatures, we next treated the cells with selective endocytosis inhibitors, both to generally confirm endocytosis, as well as reveal the specific pathways involved in uptake. Endocytosis can occur through different pathways, mediated by different factors. Clathrin-mediated endocytosis occurs through ligand-receptor recognition; the cargo is packaged into vesicles, and enters the cell with the aid of a clathrin coat [36]. Caveolae-mediated endocytosis, unlike clathrin-mediated endocytosis, is one type of receptor-independent endocytosis in which internalization through caveolae is a triggered event involving complex signaling [37]. Fluid-phase pinocytosis is another nonspecific process, characterized by bulk uptake of solutes in exact proportion to their concentration in the extracellular fluid [38].

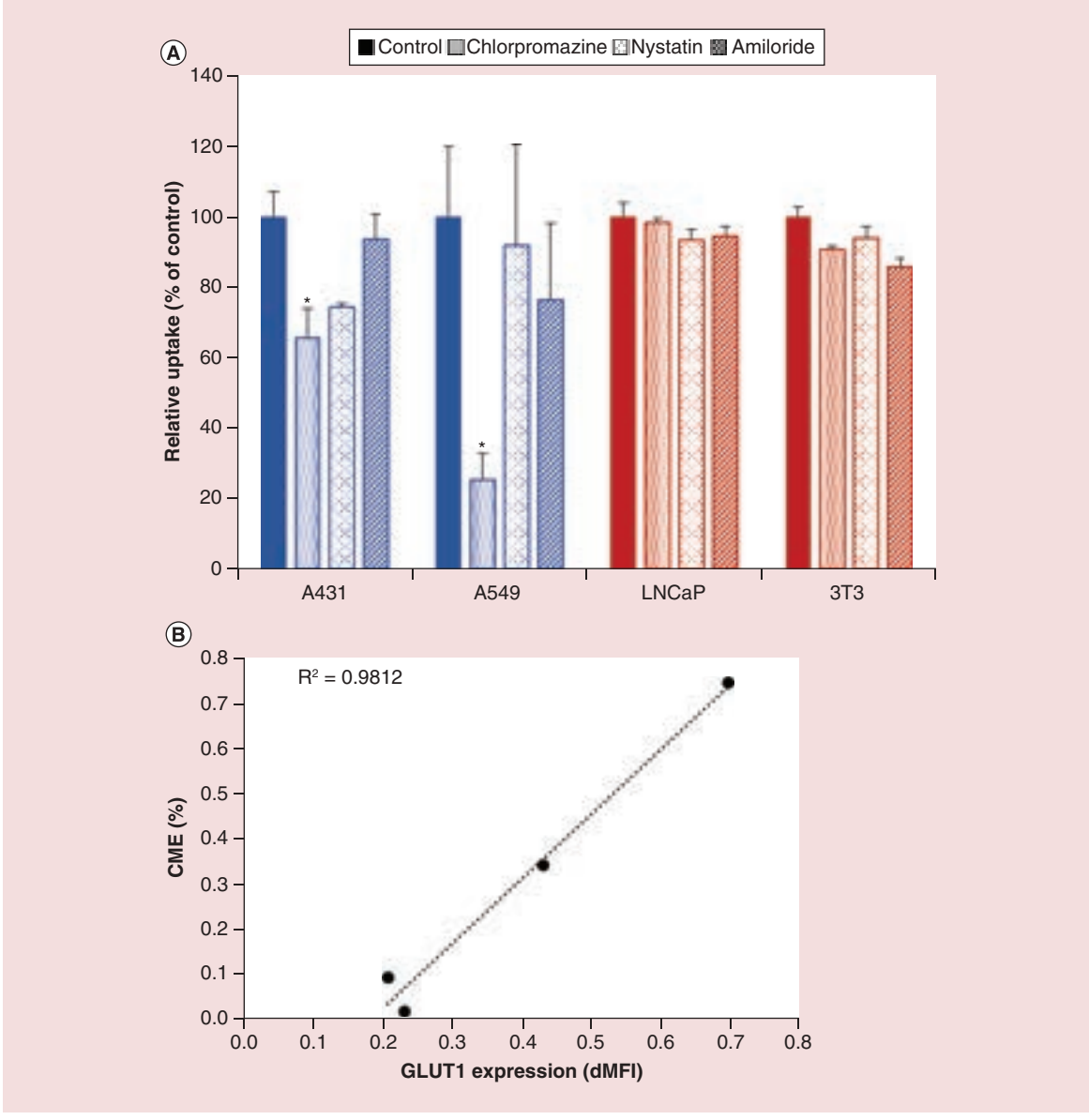

Figure 8. Effect of endocytosis inhibitors on 2-glucose-functionalized nanoparticle internalization. (A) 2-Glucose-functionalized nanoparticles (2GF-GNPs) were incubated with high (blue bars) and low (red bars) GLUT-1-expressing cells, which were pretreated with either chlorpromazine (inhibitor of clathrin-mediated endocytosis), nystatin (inhibitor of caveolae-mediated endocytosis) or amiloride (inhibitor of fluid-phase pinocytosis). Uptake of 2GF-GNPs without inhibitors was expressed as 100% and defined as control. Results presented as mean ± standard error of the mean (n = 3). *$p < 0.05$; one-way analysis of variance followed by Bonferroni's *post hoc*. **(B)** Correlation between GLUT-1 expression on the cell types and percentage of reduction in uptake induced by the clathrin-mediated endocytosis inhibitor. Mean fluorescence intensity (MFI) derived from fluorescence histogram was used to find the level of cell surface GLUT-1 expression. For comparison between the different cell lines, delta of mean fluorescence intensity (dMFI) was calculated as $(MFI_{(GLUT\text{-}1)}\text{-}MFI_{(control)})/MFI_{(control)}$. Results show that the higher the GLUT-1 surface expression, the higher the involvement of clathrin-mediated endocytosis in 2GF-GNP uptake.

Blocking of clathrin-dependent endocytosis was achieved using chlorpromazine (7 mg/ml), which causes clathrin accumulation in late endosomes, thereby inhibiting coated pit endocytosis [16]. Caveolae-mediated endocytosis was blocked using nystatin (25 mg/ml), which disruptes caveolae structures by binding cholesterol, a major caveolae component [26,39]. Fluid-phase pinocytosis was blocked using amiloride (50 μg/ml), which inhibits the Na^+/H^+ exchange required for macropinocytosis [26]. Inhibitor concentrations were determined according to the

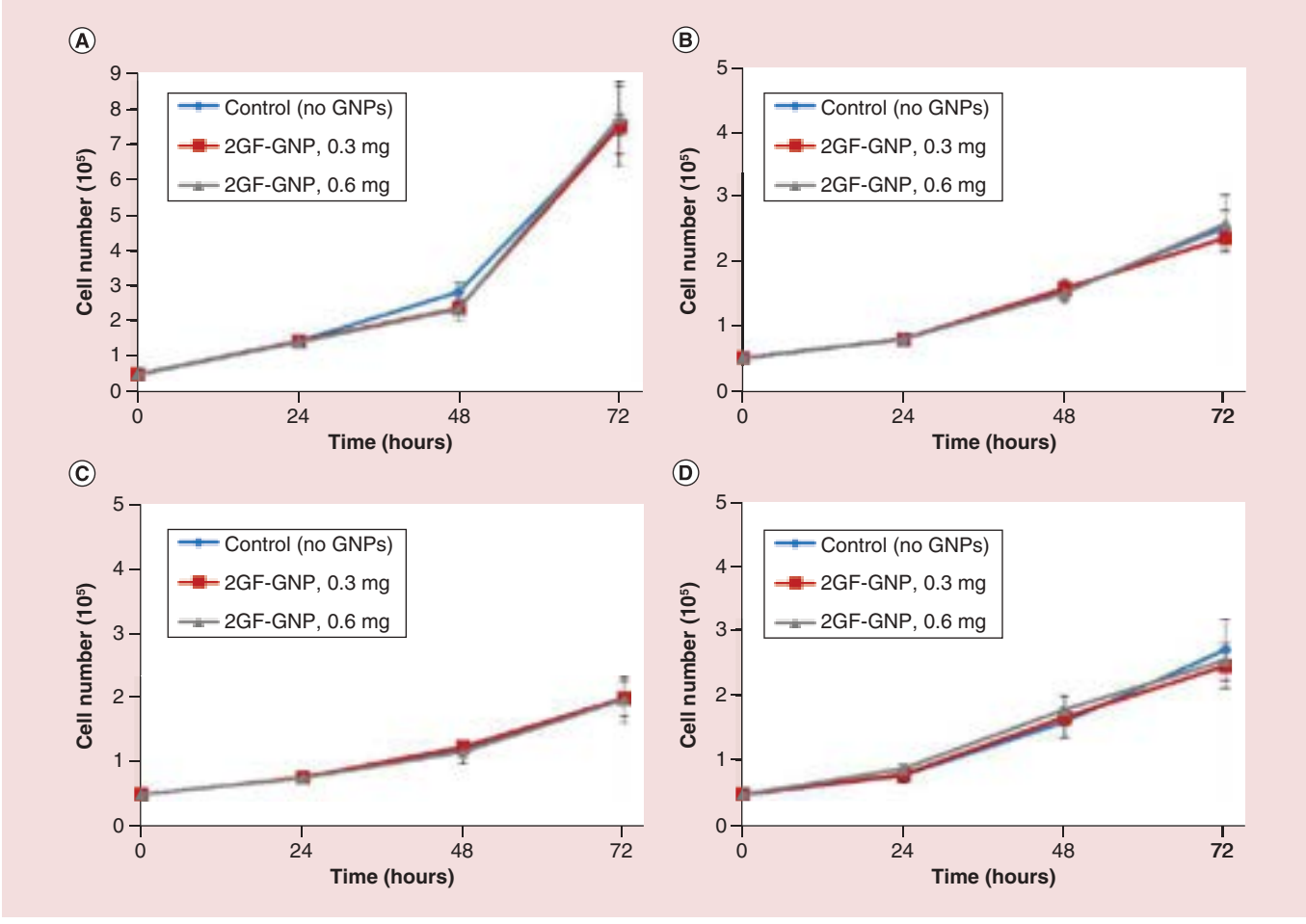

Figure 9. Cell proliferation during 72-h exposure to 2-glucose-functionalized nanoparticle. The four cell types were incubated with 2-glucose-functionalized nanoparticle at two concentrations. Cells were counted using a hemocytometer. **(A)** A431 cells **(B)** A549 cells **(C)** LNCaP cells **(D)** 3T3 cells. Results presented as mean ± standard error of the mean (n = 3).

literature [16,26]. Cells were treated with the different blockers for 1 h at 37°C, then incubated with 2GF-GNPs (30 min). Gold uptake was examined by FAAS.

We found that the cellular uptake pathway of 2GF-GNPs depends on cell type; moreover, more than one endocytic pathway can be simultaneously involved in the 2GF-GNP uptake mechanism (Figure 8A). For A431 cells, chlorpromazine and nystatin showed reduced 2GF-GNP uptake, by ~35% and ~25%, respectively, as compared with untreated control cells ($p < 0.05$ for chlorpromazine; nystatin showed a trend toward significance, $p = 0.069$). Amiloride, however, did not affect uptake in these cells. For A549 cells, chlorpromazine significantly reduced 2GF-GNP uptake by ~75% ($p < 0.05$). These results indicate that for high GLUT-1-expressing cells, clathrin-mediated endocytosis is the main mechanism involved in 2GF-GNP internalization. However, caveolae-mediated endocytosis may also be involved to a certain degree in A431 cell uptake. The lack of caveolae involvement in 2GF-GNP uptake in A549 cells concurs with the literature, which shows low expression of caveolin in A549 cells [40].

In contrast, LNCaP and 3T3 cells remained unaffected by the various inhibitors, suggesting that their low 2GF-GNP uptake occurs via different processes, which probably mainly involve diffusion.

Interestingly, we found that the involvement of clathrin-mediated endocytosis in 2GF-GNP uptake strongly correlates with GLUT-1 surface expression ($R^2 = 0.9812$; A549 gt; A431 gt; LNCaP, 3T3; Figure 8B). This implies that GLUT-1 has a major role in 2GF-GNP uptake by triggering endocytosis via the clathrin-mediated pathway.

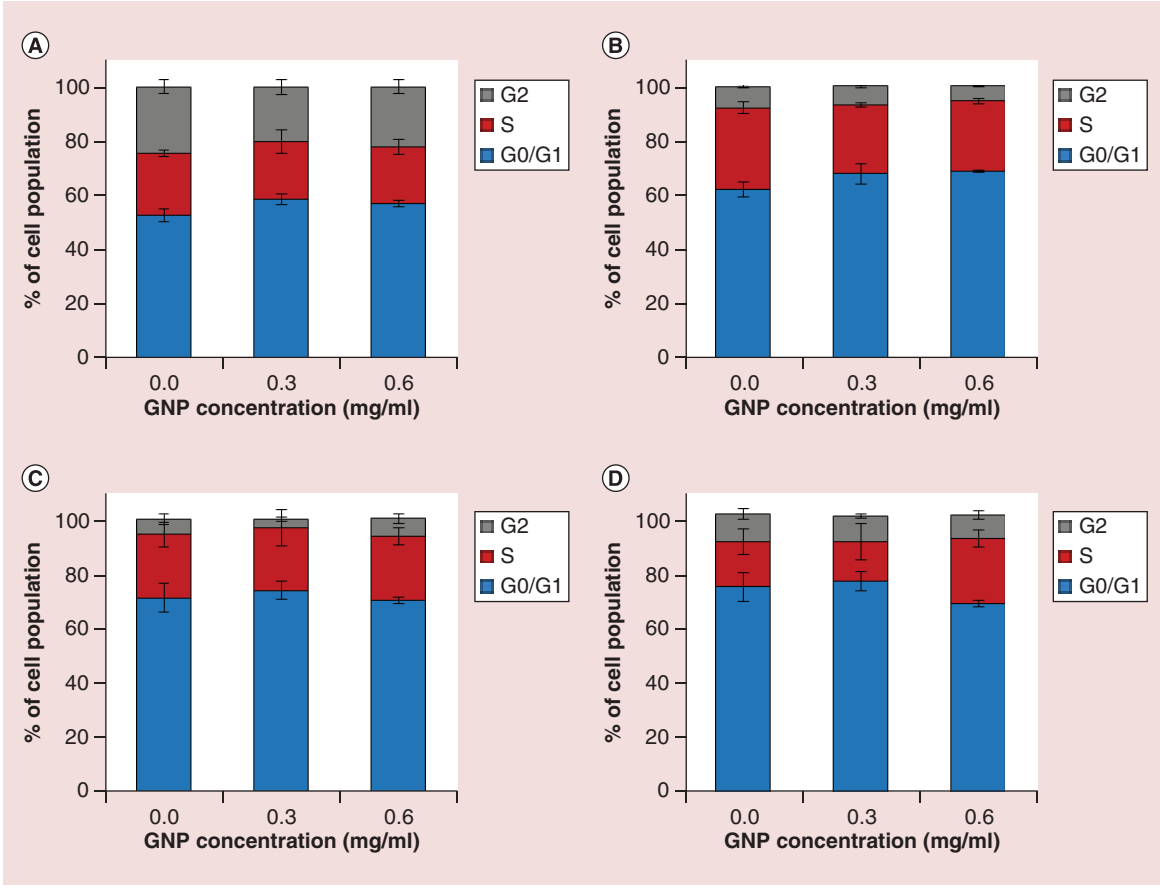

Figure 10. Cell-cycle analysis after 24 h incubation with 2-glucose-functionalized nanoparticle. Cells were incubated with 2-glucose-functionalized nanoparticle at two concentrations. Data were analyzed using flow cytometry. G0/G1, S-phase, G2 are shown in **(A)** A431 cells **(B)** A549 cells **(C)** LNCaP cells **(D)** 3T3 cells. No significant differences were found between treated cells and control, for all cell types. Result presented as mean ± standard error of the mean.

Cytotoxicity profile of 2GF-GNPs

To test the cytotoxicity profile of 2GF-GNPs, we evaluated their effect on cell proliferation and cell cycle. The four cell types were incubated with 2GF-GNPs for 72 h, and proliferation was assessed at several time points using the hemocytometer-based trypan blue dye exclusion cell quantitation and viability assay. In addition, the cells were incubated with 2GF-GNPs for 24 h, and cell cycle analysis was performed using PI staining followed by flow cytometry. After 72-h exposure to 2GF-GNPs at the concentration used above (30 mg/ml, 10 µl), as well as when increased twofold, cell proliferation remained similar to non-exposed controls, in all cell lines (Figure 9). Moreover, no significant effect on cell life cycle (G0/G1, S-phase, G2) was observed for both concentrations, in all cell lines ($p > 0.05$; Figure 10). Given that the *in vivo* use of 2GF-GNP is intended for cancer detection rather than treatment, the noncytotoxicity of 2GF-GNP is highly advantageous.

Conclusion

In the present study, we investigated the uptake mechanism and cytotoxicity profile of glucose-functionalized GNPs in different representative cell lines, namely, the high GLUT-1-expressing cells A431 head and neck squamous cell carcinoma and A549 non-small-cell lung carcinoma, and the low GLUT-1-expressing cells LNCaP prostate adenocarcinoma and 3T3 fibroblasts. We found that the cellular uptake of 2GF-GNP, but not 1GF-GNP, strongly depends on GLUT-1 surface expression. The increased uptake of 2GF-GNP by cancer cells is likely based on high glucose consumption, similar to FDG, which is also taken up by GLUT-1. This suggests that 2GF-GNPs can serve as an effective metabolically targeted agent, alternative to FDG, for many cancer types exhibiting high

overexpression of GLUT-1. Future studies should examine this approach in various animal models of high-GLUT-1 expressing tumors, in addition to its proven *in vivo* efficacy for head and neck tumors [6].

We further show that the internalization of 2GF-GNPs into high GLUT-1-expressing cells occurs mainly through clathrin-mediated endocytosis, triggered by interaction with GLUT-1. This in addition to the basal, nonspecific internalization of 2GF-GNPs, this also occurs in low GLUT-1-expressing cells. Moreover, we show that 2GF-GNPs are noncytotoxic, as they do not impair viability and cell cycle processes of the different cells.

In conclusion, this study provides fundamental insights into the uptake mechanism of glucose-functionalized GNPs. The results of this study suggest that our technology for metabolic-targeted imaging of cancer can provide a reliable and highly effective alternative to FDG, and may allow specific cancer detection in a wide range of tumors with high metabolic profiles. These findings can also advance the development of glucose-based nanoparticle systems for many other diagnostic and therapeutic applications.

Future perspective

The findings described in this paper are crucial for further development of GF-GNP-based technology for metabolic-based cancer imaging. Although this study showed no cytotoxicity of 2GF-GNP, its long-term *in vivo* toxicity and full clearance mechanism should be extensively investigated before implementing this platform in the clinic. However, despite these issues have yet to be addressed, 2GF-GNP appears to have a high potential as a promising future alternative to FDG.

Summary points

- A total of 20 nm gold nanoparticles (GNP) were synthesized and coated with glucose, by conjugation through its second or first carbon position, to yield 2-glucose-functionalized nanoparticle (2GF-GNP) or control particle 1-glucose-functionalized GNP (1GF-GNP), respectively.
- Qualitative experiments showed that 2GF-GNPs were rapidly internalized into different cell types, without penetrating the nuclei.
- GLUT-1 surface expression in the different cell types was measured and quantitative experiments were performed in order to examine a possible correlation between GF-GNP uptake and GLUT-1 expression.
- We found a strong correlation between 2GF-GNP uptake and GLUT-1 expression, while control particle, 1GF-GNP, showed very low correlation with GLUT-1 expression.
- GLUT-1 inhibition experiments demonstrated significant involvement of GLUT-1 in 2GF-GNP uptake only within high-GLUT-1 expressing cells. In contrast, 1GF-GNP uptake was not affected by GLUT-1 inhibition in all cell types.
- Endocytosis blocking experiments revealed that the main internalization pathway of 2GF-GNP is the clathrin-mediated endocytosis, which is triggered by specific interaction between 2GF-GNP and GLUT-1.
- The cytotoxicity profile of 2GF-GNPs was evaluated. No toxic effect of 2GF-GNPs on cell proliferation and cell life cycle was observed.
- The results indicate a direct association between the underlying mechanisms of our nanoparticle-based technology and those of fluorodeoxyglucose-PET. Therefore, 2GF-GNP can provide a reliable alternative to 2-[18 F]-2-Deoxy-D-Glucose, and may allow specific cancer detection in a wide range of tumors with high metabolic profiles.

Supplementary Materials

A Supplementary video is available as an accompaniment to this paper. To view the Supplementary video, please visit the journal website at: www.futuremedicine.com/doi/full/10.2217/nnm-2018-0022

The video shows time-lapse imaging of the cellular uptake of 2GF-GNP marked with rhodamine B into A431 cells.

Supplementary Figures and Methods are also available to view here: www.futuremedicine.com/doi/suppl/10.2217/nnm-2018-0022

Acknowledgements

This work was partially supported bythe Israel Science Foundation grant (749/14), by the Israel Cancer Research Fund (ICRF), by the Leon and Maria Taubenblatt Prize for Excellence in Medical Research and by the doctoral scholarship granted to T.D. by the Ministry of Science & Technology, Israel.

Financial & competing interests disclosure

The authors have no relevant affiliations or financial involvement with any organization or entity with a financial interest in or financial conflict with the subject matter or materials discussed in the manuscript. This includes employment, consultancies, honoraria, stock ownership or options, expert testimony, grants or patents received or pending, or royalties.

No writing assistance was utilized in the production of this manuscript.

References

1. Mout R, Moyano DF, Rana S, Rotello VM. Surface functionalization of nanoparticles for nanomedicine. *Chem. Soc. Rev.* 41(7), 2539–2544 (2012).
2. Katz E, Willner I. Integrated nanoparticle – biomolecule hybrid systems: synthesis, properties, and applications. *Angew. Chemie Int. Ed.* 43, 6042–6108 (2004).
3. Dreifuss T, Betzer O, Shilo M, Popovtzer A, Motiei M, Popovtzer R. A challenge for theranostics: is the optimal particle for therapy also optimal for diagnostics? *Nanoscale* 7, 15175–15184 (2015).
4. Jin J, Park H, Zhang W *et al.* Biomaterials Modular delivery of CpG-incorporated lipid-DNA nanoparticles for spleen DC activation. *Biomaterials* 115, 81–89 (2017).
5. El-boubbou K, Huang X. Glyco-nanomaterials: translating insights from the "sugar-code" to biomedical applications. *Curr. Med. Chem.* 18, 2060–2078 (2011).
6. Motiei M, Dreifuss T, Betzer O *et al.* Differentiating between cancer and inflammation: a metabolic-based method for functional computed tomography imaging. *ACS Nano* 10(3), 3469–3477 (2016).
7. Liberti MV, Locasale JW. The Warburg effect: how does it benefit cancer cells? *Trends Biochem. Sci.* 41(3), 211–218 (2017).
8. Asik E, Aslan Tuğba Nur, Volkan M, Güray N Tülin. 2-amino-2-deoxy-glucose conjugated cobalt ferrite magnetic nanoparticle (2DG-MNP) as a targeting agent for breast cancer cells. *Environ. Toxicol. Pharmacol.* 41, 272–278 (2016).
9. Barbaro D, Bari L Di, Gandin V *et al.* Glucose-coated superparamagnetic iron oxide nanoparticles prepared by metal vapour synthesis are electively internalized in a pancreatic adenocarcinoma cell line expressing GLUT1 transporter. *PLoS ONE* 10(4), 1–13 (2015).
10. Li J, Ma FK, Dang QF, Liang XG, Chen XG. Glucose-conjugated chitosan nanoparticles for targeted drug delivery and their speci fi c interaction with tumor cells. *Front. Mater. Sci.* 8(4), 363–372 (2014).
11. Venturelli L, Nappini S, Bulfon M *et al.* Glucose is a key driver for GLUT1-mediated nanoparticles internalization in breast cancer cells. *Sci. Rep.* 6, 1–14 (2016).
12. Brown RS, Leung JY, Kison PV, Zasadny KR, Flint A, Wahl RL. Glucose transporters and FDG uptake in untreated primary human non-small-cell lung cancer. *J. Nucl. Med.* 40(4), 556–565 (1999).
13. Higashi K, Ueda Y, Sakurai A *et al.* Correlation of GLUT-1 glucose transporter expression with [(18)F]FDG uptake in non-small-cell lung cancer. *Eur. J. Nucl. Med.* 27(12), 1778–1785 (2000).
14. Kato H, Takita J, Miyazaki T *et al.* Correlation of 18-F-fluorodeoxyglucose (FDG) accumulation with glucose transporter (GLUT-1) expression in esophageal squamous cell carcinoma. *Anticancer Res.* 23(4), 3263–3272 (2003).
15. Iversen T, Skotland T, Sandvig K. Endocytosis and intracellular transport of nanoparticles: present knowledge and need for. *Nano Today* 6(2), 176–185 (2011).
16. Jiang L, Li X, Liu L, Zhang Q. Cellular uptake mechanism and intracellular fate of hydrophobically modified pullulan nanoparticles. *Int. J. Nanomedicine* 8, 1825–1834 (2013).
17. Gu YMÆH. Study on the endocytosis and the internalization mechanism of aminosilane-coated Fe_3O_4 nanoparticles *in vitro*. *J. Mater. Sci. Mater. Med.* 18(11), 2145–2149 (2007).
18. Jones AT, Gumbleton M, Duncan R. Understanding endocytic pathways and intracellular trafficking: a prerequisite for effective design of advanced drug delivery systems. *Adv. Drug Deliv. Rev.* 55, 1353–1357 (2003).
19. Jordan A, Scholz R, Wust P *et al.* Endocytosis of dextran and silan-coated magnetite nanoparticles and the effect of intracellular hyperthermia on human mammary carcinoma cells *in vitro*. *J. Magn. Magn. Mater.* 194, 185–196 (1999).
20. Jordan A, Scholz R, Maier-hau K *et al.* Presentation of a new magnetic field therapy system for the treatment of human solid tumors with magnetic fluid hyperthermia. *J. Magn. Magn. Mater.* 225, 118–126 (2001).
21. Moore MN. Do nanoparticles present ecotoxicological risks for the health of the aquatic environment ? *Environ. Int.* 32, 967–976 (2006).
22. Enustun BV, Turkevich J. Coagulation of colloidal gold. *J. Am. Chem. Soc.* 85(21), 3317–3328 (1963).
23. Shilo M, Berenstein P, Dreifuss T *et al.* Insulin-coated gold nanoparticles as a new concept for personalized and adjustable glucose regulation. *Nanoscale* 7, 20489–20496 (2015).
24. Meir R, Betzer O, Motiei M, Kronfeld N, Brodie C, Popovtzer R. Design principles for noninvasive, longitudinal and quantitative cell tracking with nanoparticle-based CT imaging. *Nanomed. Nanotechnol. Biol. Med.* 13(2), 421–429 (2017).
25. Betzer O, Perets N, Angel A *et al. In vivo* neuroimaging of exosomes using gold nanoparticles. *ACS Nano.* 11(11), 10883–10893 (2017).

26. Bardor M, Nguyen DH, Diaz S, Varki A. Mechanism of uptake and incorporation of the non-human sialic acid N-glycolylneuraminic acid into human cells. *J. Biol. Chem.* 280(6), 4228–4237 (2005).
27. Mueckler M, Makepeace C. Analysis of transmembrane segment 8 of the GLUT1 glucose transporter by cysteine-scanning mutagenesis and substituted cysteine accessibility. *J. Biol. Chem.* 279(11), 10494–10499 (2004).
28. Mellanen P, Minn H, Grenman R, Harkonen P. Expression of glucose transporters in head-and-neck tumors. *Int. J. Cancer.* 56, 622–629 (1994).
29. Zhou X, Chen R, Xie W, Ni Y, Liu J, Huang G. Relationship between 18 F-FDG accumulation and lactate dehydrogenase A expression in lung adenocarcinomas. *J. Nucl. Med.* 55(11), 1766–1772 (2014).
30. Kaira K, Serizawa M, Koh Y *et al.* Lung cancer biological significance of 18 F-FDG uptake on PET in patients with non-small-cell lung cancer. *Lung Cancer* 83(2), 197–204 (2014).
31. Ong LC, Jin Y, Song IC, Yu S, Zhang K, Chow PKH. 2-[18 F]-2-deoxy-D-glucose (FDG) uptake in human tumor cells is related to the expression of GLUT-1 and hexokinase II. *Acta radiol.* 49, 1145–1153 (2008).
32. Effert P, Beniers AJ, Tamimi Y, Handt S, Jakse G. Expression of glucose transporter 1 (GLUT-1) in cell lines and clinical specimens from human prostate adenocarcinoma. *Anticancer Res.* 24, 3057–3063 (2004).
33. Koch A, Lang SA, Wild PJ *et al.* Glucose transporter isoform 1 expression enhances metastasis of malignant melanoma cells. *Oncotarget.* 6(32), 32748–32760 (2015).
34. Gottschalk I, Lundqvist A, Zeng C-M *et al.* Conversion between two cytochalasin B-binding states of the human GLUT1 glucose transporter. *Eur. J. Biochem.* 267(23), 6875–6882 (2000).
35. Pinkofsky HB, Dwyer DS, Bradley RJ. The inhibition of GLUT1 glucose transport and cytochalasin B binding activity by tricyclic antidepressants. *Life Sci.* 66(3), 271–278 (1999).
36. Mcmahon HT, Boucrot E. Molecular mechanism and physiological functions of clathrin - mediated endocytosis. *Nat. Rev. Mol. Cell Biol.* 12(8), 517–533 (2011).
37. Pelkmans L, Helenius A. Endocytosis via caveolae. *Traffic.* 3(13), 311–320 (2002).
38. Khalil IA, Kogure K, Akita H, Harashima H. Uptake pathways and subsequent intracellular trafficking in nonviral gene delivery. *Pharmacol. Rev.* 58(1), 32–45 (2006).
39. Kim S, Ph D, Han J, Lee DH, Cho KH. Cholesterol, a major component of caveolae, down-regulates matrix metalloproteinase-1 expression through ERK / JNK pathway in cultured human dermal fibroblasts. *Ann. Dermatol.* 22(4), 379–388 (2010).
40. Racine C, Be M, Hirabayashi H, Chakir J, Couet J. Reduction of *caveolin 1* gene expression in lung carcinoma cell lines. *Biochem. Biophys. Res. Commun.* 255, 580–586 (1999).